Kalman Filtering for Relative Spacecraft Attitude and Position Estimation

Son-Goo Kim,* John L. Crassidis,† Yang Cheng,‡ Adam M. Fosbury§

University at Buffalo, State University of New York, Amherst, NY 14260-4400

John L. Junkins¶

Texas A&M University, College Station, TX 77843-3141

In this paper a novel approach is developed for relative state estimation of spacecraft flying in formation. The approach uses information from an optical sensor to provide multiple line-of-sight vectors from one spacecraft to another. The line-of-sight measurements are coupled with gyro measurements and dynamical models in an extended Kalman filter to determine relative attitude, position and gyro biases. The quaternion is used to describe the relative kinematics, while general relative orbital equations are used to describe the positional dynamics. Three different attitude formulations are

*Graduate Student, Department of Mechanical & Aerospace Engineering. Currently Researcher, Attitude and Orbit Control Team, Satellite Division, SaTReC, KAIST, 373-1 Kusong-dong, Yusong-gu, Taejon 305-701, Republic Korea. Email: songoo@satrec.kaist.ac.kr. Member AIAA.

†Associate Professor, Department of Mechanical & Aerospace Engineering. Email: johnc@eng.buffalo.edu. Associate Fellow AIAA.

‡Postdoctoral Research Fellow, Department of Mechanical & Aerospace Engineering. Email: cheng3@eng.buffalo.edu. Member AIAA.

§Graduate Student, Department of Mechanical & Aerospace Engineering. Email: fosbury@eng.buffalo.edu. Student Member AIAA.

¶George J. Eppright Chair Professor, Department of Aerospace Engineering. Email: junkins@tamu.edu. Fellow AIAA.

presented. The first estimates the relative attitude and individual gyro biases for the chief and deputy spacecraft. The second estimates the relative attitude, and the relative velocity bias and the deputy gyro bias. The third estimates the relative attitude, and the relative velocity bias and the chief gyro bias. Simulation results indicate that the combined sensor/estimator approach provides accurate relative attitude and position estimates.

I. Introduction

Spacecraft formation flying is an important technology, but not a new concept anymore.[1,2] Since the early days of the space program several formation flying applications, such as rendezvous and docking maneuvers, have been accomplished in practice. Modern day spacecraft formation flying applications include long baseline interferometry, stereographic imaging, synthetic apertures, and distinguishing spatial from temporal magnetospheric variations. Many missions, in particular interferometry missions, rely on precise relative attitude and position knowledge in order to maintain mission requirements. To date most research studies into determining relative attitudes and positions between vehicles have involved using the Global Positioning System (GPS),[3] which restricts the spacecraft formation to near-Earth applications. An application of GPS-like technology to a deep space mission has been proposed,[4] but this requires extensive hardware development and is subject to the generic GPS performance-limiting effects, including multipath, geometric dilution of precision, integer ambiguity resolution and cycle slip. An objective of this paper is to provide a novel, reliable and autonomous relative attitude and position estimation system that is independent of any external systems.

The relative sensor measurements used in this paper are line-of-sight (LOS) vectors between two spacecraft. These can be obtained from a vision-based navigation (VISNAV) system, which comprises an optical sensor of a new kind combined with specific light sources (beacons) in order to achieve a selective or "intelligent" vision. The sensor is made up of a Position Sensing Diode (PSD) placed in the focal plane of a wide angle lens. Benefits of this

configuration include: 1) very small sensor size, 2) very wide sensor field-of-view (FOV), 3) no complex/time consuming charge-coupling-device signal processing or pattern recognition required, 4) excellent rejection of ambient light interference under a wide variety of operating conditions, and 5) relatively simple electronic circuits with modest digital signal processing micro-computer requirements. A more detailed description of the VISNAV system can be found in Ref. 5.

This paper presents an extended Kalman filter (EKF) formulation to estimate the relative attitude and position of two spacecraft using LOS observations coupled with gyro measurements from each spacecraft. The attitude kinematics are based on the quaternion. Three different formulations are presented. The first estimates the relative attitude and individual gyro biases for the chief and deputy spacecraft. The second estimates the relative attitude, and the relative velocity bias and the deputy gyro bias. The third estimates the relative attitude, and the relative velocity bias and the chief gyro bias. The analysis of relative position motion of spacecraft also has been a key issue for planning formation flying and orbital rendezvous missions. In the early 1960's, Clohessy and Wiltshire (CW) formulated a set of simple linear relative equations of motion, derived by assuming small deviations from a circular reference orbit with no perturbations.[6,7] Others have generalized the CW equations for eccentric reference orbits,[8] and to include perturbations and higher-order nonlinear effects.[9] Another interesting approach formulates the relative motion in spherical coordinates in order to derive second-order expressions.[10] In this paper the nonlinear relative equations of motions use Cartesian components with no external disturbances.[11] Other formulations that include disturbances can be easily derived if necessary.

The organization of this paper proceeds as follows. First, an overview of the relative coordinates systems and positional equations of motion is given. Then, the basic equations for the VISNAV system and gyro models are shown. Next, a review of the quaternion kinematics is provided, followed by a derivation of the relative attitude motion equations. Next, an EKF is derived for attitude estimation only, which assumes that the relative positions are known. Then, the relative position equations are appended to the state vector in order

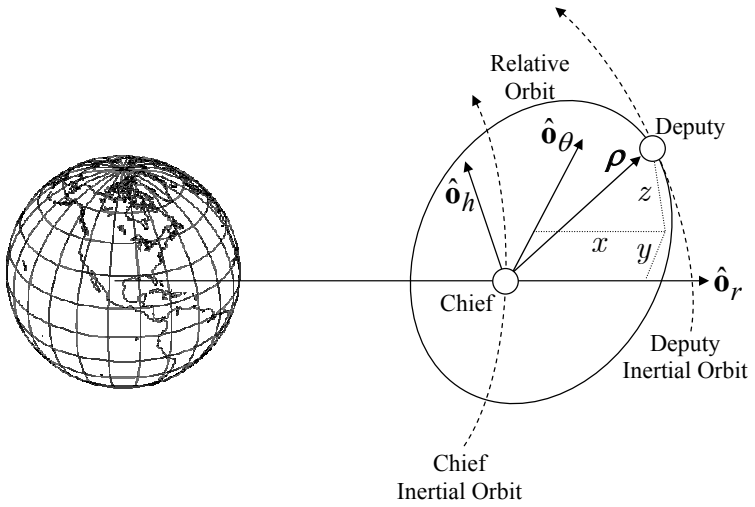

Figure 1. General Type of Spacecraft Formation with Relative Motion

to perform full attitude and position estimation. Finally, simulation results are presented.

II. Overview

In this section an overview of the frames used to describe the relative attitude and position equations of motion is shown. The measurement equations for the VISNAV sensor, which provides LOS vectors from one spacecraft to another, are then derived. Also, standard gyro measurement equations are shown, which will be used for relative attitude estimation.

A. Relative Orbital Motion Equations

The spacecraft about which all other spacecraft are orbiting is referred to as the chief. The remaining spacecraft are referred to as the deputies. The relative orbit position vector, $\boldsymbol{\rho}$, is expressed in components by $\boldsymbol{\rho} = [x \;\; y \;\; z]^T$, shown in Figure 1. The vector triad $\{\hat{\mathbf{o}}_r, \hat{\mathbf{o}}_\theta, \hat{\mathbf{o}}_h\}$ is known as the Hill coordinate frame, where $\hat{\mathbf{o}}_r$ is in the orbit radius direction, $\hat{\mathbf{o}}_h$ is parallel with the orbit momentum vector and $\hat{\mathbf{o}}_\theta$ completes the triad. A complete derivation of the relative equations of motion for eccentric orbits can be found in Ref. 11. If the relative orbit coordinates are small compared to the chief orbit radius, then the equations of motion are

given by

$$\ddot{x} - x\,\dot{\theta}^2\left(1 + 2\frac{r_c}{p}\right) - 2\,\dot{\theta}\left(\dot{y} - y\frac{\dot{r}_c}{r_c}\right) = w_x \tag{1a}$$

$$\ddot{y} + 2\,\dot{\theta}\left(\dot{x} - x\frac{\dot{r}_c}{r_c}\right) - y\,\dot{\theta}^2\left(1 - \frac{r_c}{p}\right) = w_y \tag{1b}$$

$$\ddot{z} + z\,\dot{\theta}^2\frac{r_c}{p} = w_z \tag{1c}$$

where p is semilatus rectum of the chief, r_c is the chief orbit radius and $\dot{\theta}$ is true anomaly rate of the chief. Also, w_x, w_y and w_z are acceleration disturbances which are modeled as zero-mean Gaussian white-noise processes, with variances given by σ_x^2, σ_y^2 and σ_z^2, respectively. The true anomaly acceleration and chief orbit-radius acceleration are given by

$$\ddot{\theta} = -2\frac{\dot{r}_c}{r_c}\dot{\theta} \tag{2a}$$

$$\ddot{r}_c = r_c\,\dot{\theta}^2\left(1 - \frac{r_c}{p}\right) \tag{2b}$$

If the chief satellite orbit is assumed to be circular so that $\dot{r}_c = 0$ and $p = r_c$, then the relative equations of motion reduce to the simple form known as the CW equations (with disturbances added here):

$$\ddot{x} - 2\,n\,\dot{y} - 3\,n^2 x = w_x \tag{3a}$$

$$\ddot{y} + 2\,n\,\dot{x} = w_y \tag{3b}$$

$$\ddot{z} + n^2 z = w_z \tag{3c}$$

where $n = \dot{\theta}$ is the mean motion.

B. Vision-Based Navigation System and Gyro Model

Photogrammetry is the technique of measuring objects (2D or 3D) from photographic images or LOS measurements. Photogrammetry can generally be divided into two categories: far range photogrammetry with camera distance settings to infinity (commonly used in star

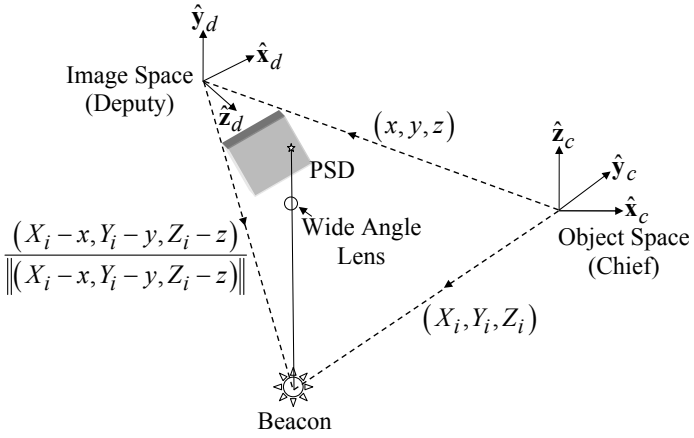

Figure 2. Vision-Based Navigation System

cameras[12]), and close-range photogrammetry with camera distance settings to finite values. In general close-range photogrammetry can be used to determine both the attitude and position of an object, while far range photogrammetry can only be used to determine attitude. The VISNAV system comprises an optical sensor of a new kind combined with specific light sources (beacons), which can be used for close-range photogrammetry-type applications. The relationship between the attitude/position and the observations used in photogrammetry involves a set of colinearity equations, which are reviewed in this section. Figure 2 shows a schematic of the typical quantities involved in basic photogrammetry from LOS measurements, derived from light beacons in this case. It is assumed that the location of the sensor focal plane is known within the deputy spacecraft coordinate system, which is usually obtained through calibration. Without loss in generality, we assume that the chief spacecraft frame coincides with the Hill frame describe in Figure 1. If we choose the z-axis of the sensor coordinate system to be directed outward along the boresight, then given object space and image space coordinate frames (see Figure 2), the ideal object to image space projective transformation (noiseless) can be written as follows:[13]

$$\chi_i = -f \frac{A_{11}(X_i - x) + A_{12}(Y_i - y) + A_{13}(Z_i - z)}{A_{31}(X_i - x) + A_{32}(Y_i - y) + A_{33}(Z_i - z)}, \quad i = 1, 2, \ldots, N \tag{4a}$$

$$\gamma_i = -f \frac{A_{21}(X_i - x) + A_{22}(Y_i - y) + A_{23}(Z_i - z)}{A_{31}(X_i - x) + A_{32}(Y_i - y) + A_{33}(Z_i - z)}, \quad i = 1, 2, \ldots, N \tag{4b}$$

where N is the total number of observations, (χ_i, γ_i) are the image space observations for the i^{th} LOS, (X_i, Y_i, Z_i) are the known object space locations of the i^{th} beacon, (x, y, z) are the unknown object space location of the sensor modeled by Eq. (1), f is the known focal length, and A_{jk} are the unknown coefficients of the attitude matrix, A, associated to the orientation from the object plane (chief) to the image plane (deputy). The goal of the *inverse problem* is given observations (χ_i, γ_i) and object space locations (X_i, Y_i, Z_i), for $i = 1, 2, \ldots, N$, determine the attitude (A) and position (x, y, z).

The observation can be reconstructed in unit vector form as

$$\mathbf{b}_i = A\mathbf{r}_i, \quad i = 1, 2, \ldots, N \tag{5}$$

where

$$\mathbf{b}_i \equiv \frac{1}{\sqrt{f^2 + \chi_i^2 + \gamma_i^2}} \begin{bmatrix} -\chi_i \\ -\gamma_i \\ f \end{bmatrix} \tag{6a}$$

$$\mathbf{r}_i \equiv \frac{1}{\sqrt{(X_i - x)^2 + (Y_i - y)^2 + (Z_i - z)^2}} \begin{bmatrix} X_i - x \\ Y_i - y \\ Z_i - z \end{bmatrix} \tag{6b}$$

When measurement noise is present, the measurement model becomes

$$\tilde{\mathbf{b}}_i = A\mathbf{r}_i + \boldsymbol{\upsilon}_i \tag{7}$$

where $\tilde{\mathbf{b}}_i$ denotes the i^{th} measurement, and the sensor error $\boldsymbol{\upsilon}_i$ is approximately Gaussian

which satisfies[14]

$$E\{\boldsymbol{v}_i\} = \mathbf{0} \tag{8a}$$

$$\mathcal{R}_i \equiv E\left\{\boldsymbol{v}_i \boldsymbol{v}_i^T\right\} = J_i\, R_i^{\text{FOCAL}} J_i^T \tag{8b}$$

where $E\{\,\}$ denotes expectation and

$$J_i \equiv \frac{1}{\sqrt{1+\chi_i^2+\gamma_i^2}} \begin{bmatrix} -1 & 0 \\ 0 & -1 \\ 0 & 0 \end{bmatrix} - \frac{1}{1+\chi_i^2+\gamma_i^2} \mathbf{b}_i \begin{bmatrix} \chi_i & \gamma_i \end{bmatrix} \tag{9a}$$

$$R_i^{\text{FOCAL}} = \frac{\sigma_i^2}{1+d\,(\chi_i^2+\gamma_i^2)} \begin{bmatrix} (1+d\,\chi_i^2)^2 & (d\,\chi_i\gamma_i)^2 \\ (d\,\chi_i\gamma_i)^2 & (1+d\,\gamma_i^2)^2 \end{bmatrix} \tag{9b}$$

where σ_i^2 is the variance of the measurement errors associated with χ_i and γ_i, and d is on the order of one. Note that as χ_i or γ_i increases then the individual components of R_i^{FOCAL} increase, which realistically shows that the errors increase as the observation moves away from the boresight. As stated in Ref. 15, the covariance model is a function of the true variables χ_i and γ_i, which are never available in practice. However, using the measurements themselves or estimated quantities from the EKF leads to only second-order error effects.

Equation (8) does not make the small FOV assumption, which is more useful for the VISNAV sensor since it incorporates a wide angle lens. Rather, the assumption leading to Eq. (8) is that the measurement noise is "small" compared to the signal, so that a first-order Taylor series expansion accurately captures the error process (see Ref. 14 for details). However, there may be circumstances where all the LOS measurements are within a small FOV. For this case Shuster[16] has shown that nearly all the probability of the errors is concentrated on a very small area about the direction of $A\mathbf{r}_i$, so the sphere containing that

point can be approximated by a tangent plane, characterized by

$$E\{\boldsymbol{v}_i\} = \mathbf{0} \tag{10a}$$

$$\mathcal{R}_i = \sigma_i^2 \left(I_{3\times 3} - \mathbf{b}_i \mathbf{b}_i^T\right) \tag{10b}$$

where $I_{3\times 3}$ denotes a 3×3 identity matrix. Equation (10b) approximates Eq. (8b) well under the small FOV assumption, but can lead to fairly large estimation errors if this assumption is not valid.[14]

The covariance matrices in Eqs. (8b) and (10b) are both singular, which leads to a singularity in the calculation of the Kalman gain. Shuster[15] first showed that the singular covariance matrix in Eq. (10b) can be effectively replaced with a nonsingular diagonal matrix made up of σ_i^2 terms. This concept is expanded in Ref. 14 to include the general covariance shown by Eq. (8b). For each measurement, the matrix used to make up the EKF measurement-error covariance matrix is given by a rank-one update to $\mathcal{R}_i$:

$$R_i = \mathcal{R}_i + \frac{1}{2}\text{trace}(\mathcal{R}_i)\mathbf{b}_i\mathbf{b}_i^T \tag{11}$$

This matrix is always nonsingular.[14] If Eq. (10b) is used in Eq. (11) then we have $R_i = \sigma_i^2 I_{3\times 3}$. Finally, concatenating all R_i matrices for the available LOS measurements at time-step t_k into a block diagonal matrix leads to the EKF measurement covariance matrix, denoted by R_k.

A common sensor that measures the angular velocity is a rate-integrating gyro. For this sensor, a widely used model is given by[17]

$$\tilde{\boldsymbol{\omega}} = \boldsymbol{\omega} + \boldsymbol{\beta} + \boldsymbol{\eta}_v \tag{12a}$$

$$\dot{\boldsymbol{\beta}} = \boldsymbol{\eta}_u \tag{12b}$$

where $\boldsymbol{\omega}$ is the continuous-time true angular velocity, $\tilde{\boldsymbol{\omega}}$ is the measured velocity, $\boldsymbol{\beta}$ is the

drift, and $\boldsymbol{\eta}_v$ and $\boldsymbol{\eta}_u$ are independent zero-mean Gaussian white-noise processes with

$$E\left\{\boldsymbol{\eta}_v(t)\boldsymbol{\eta}_v^T(\tau)\right\} = I_{3\times3}\sigma_v^2\delta(t-\tau) \tag{13a}$$

$$E\left\{\boldsymbol{\eta}_u(t)\boldsymbol{\eta}_u^T(\tau)\right\} = I_{3\times3}\sigma_u^2\delta(t-\tau) \tag{13b}$$

where $\delta(t-\tau)$ is the Dirac delta function. In this paper we use ($\boldsymbol{\eta}_{cv}$, $\boldsymbol{\eta}_{cu}$) and ($\boldsymbol{\eta}_{dv}$, $\boldsymbol{\eta}_{du}$) to denote the parameters of chief and deputy gyros, respectively. It is important to note that gyros measure with respect to an inertial frame, not with respect to the frames used to the describe the chief and deputy spacecraft shown in this section.

III. Relative Attitude Kinematics

In this section a brief review of the attitude kinematics equation of motion using the quaternion is shown, as well as some useful identities. Then, the relative attitude kinematics equation between two spacecraft is shown, followed by a closed-form solution of the relative state transition matrix.

A. Quaternion Kinematics

In this section a brief review of the quaternion kinematics is shown. More details are given in Ref. 18. The quaternion is defined by $\mathbf{q} \equiv \begin{bmatrix}\boldsymbol{\varrho}^T & q_4\end{bmatrix}^T$, with $\boldsymbol{\varrho} \equiv \begin{bmatrix}q_1 & q_2 & q_3\end{bmatrix}^T = \hat{\mathbf{e}}\sin(\vartheta/2)$ and $q_4 = \cos(\vartheta/2)$, where $\hat{\mathbf{e}}$ is the axis of rotation and ϑ is the angle of rotation.[18] Since a four-dimensional vector is used to describe three dimensions, the quaternion components cannot be independent of each other. The quaternion satisfies a single constraint given by $||\mathbf{q}|| = 1$. The attitude matrix is related to the quaternion by

$$A(\mathbf{q}) = \Xi^T(\mathbf{q})\Psi(\mathbf{q}) \tag{14}$$

with

$$\Xi(\mathbf{q}) \equiv \begin{bmatrix} q_4 I_{3\times 3} + [\boldsymbol{\varrho}\times] \\ -\boldsymbol{\varrho}^T \end{bmatrix} \tag{15a}$$

$$\Psi(\mathbf{q}) \equiv \begin{bmatrix} q_4 I_{3\times 3} - [\boldsymbol{\varrho}\times] \\ -\boldsymbol{\varrho}^T \end{bmatrix} \tag{15b}$$

where $[\boldsymbol{\varrho}\times]$ is a cross product matrix since $\mathbf{a}\times\mathbf{b} = [\mathbf{a}\times]\mathbf{b}$, with

$$[\mathbf{a}\times] \equiv \begin{bmatrix} 0 & -a_3 & a_2 \\ a_3 & 0 & -a_1 \\ -a_2 & a_1 & 0 \end{bmatrix} \tag{16}$$

Successive rotations can be accomplished using quaternion multiplication. Here we adopt the convention of Ref. [19] who multiply the quaternions in the same order as the attitude matrix multiplication: $A(\mathbf{q}')A(\mathbf{q}) = A(\mathbf{q}'\otimes\mathbf{q})$. The composition of the quaternions is bilinear, with

$$\mathbf{q}'\otimes\mathbf{q} = \Big[\Psi(\mathbf{q}') \ \vdots \ \mathbf{q}'\Big]\,\mathbf{q} = \Big[\Xi(\mathbf{q}) \ \vdots \ \mathbf{q}\Big]\,\mathbf{q}' \tag{17}$$

The inverse quaternion is given by $\mathbf{q}^{-1} = \begin{bmatrix} -\boldsymbol{\varrho}^T & q_4 \end{bmatrix}^T$. Note that $\mathbf{q}\otimes\mathbf{q}^{-1} = [0\ 0\ 0\ 1]^T$, which is the identity quaternion.

The quaternion kinematics equation is given by

$$\dot{\mathbf{q}} = \frac{1}{2}\Xi(\mathbf{q})\boldsymbol{\omega} = \frac{1}{2}\Omega(\boldsymbol{\omega})\mathbf{q} \tag{18}$$

where

$$\Omega(\boldsymbol{\omega}) \equiv \begin{bmatrix} -[\boldsymbol{\omega}\times] & \boldsymbol{\omega} \\ -\boldsymbol{\omega}^T & 0 \end{bmatrix} \tag{19}$$

Some useful identities are given by

$$\Xi^T(\mathbf{q})\Xi(\mathbf{q}) = \Psi^T(\mathbf{q})\Psi(\mathbf{q}) = I_{3\times 3} \tag{20a}$$

$$\Xi(\mathbf{q})\Xi^T(\mathbf{q}) = \Psi(\mathbf{q})\Psi^T(\mathbf{q}) = I_{4\times 4} - \mathbf{q}\,\mathbf{q}^T \tag{20b}$$

$$\Xi^T(\mathbf{q})\mathbf{q} = \Psi^T(\mathbf{q})\mathbf{q} = \mathbf{0}_{3\times 1} \tag{20c}$$

$$\begin{bmatrix} \boldsymbol{\omega} \\ 0 \end{bmatrix} \otimes \mathbf{q} = \Omega(\boldsymbol{\omega})\mathbf{q} \tag{20d}$$

$$\mathbf{q} \otimes \begin{bmatrix} \boldsymbol{\omega} \\ 0 \end{bmatrix} = \Gamma(\boldsymbol{\omega})\mathbf{q} \tag{20e}$$

$$\Psi(\mathbf{q})\boldsymbol{\omega} = \Gamma(\boldsymbol{\omega})\mathbf{q} \tag{20f}$$

where

$$\Gamma(\boldsymbol{\omega}) \equiv \begin{bmatrix} [\boldsymbol{\omega}\times] & \boldsymbol{\omega} \\ -\boldsymbol{\omega}^T & 0 \end{bmatrix} \tag{21}$$

It is assumed in Eqs. (20a) and (20b) that $||\mathbf{q}|| = 1$. Also, $\Omega(\mathbf{a})$ and $\Gamma(\mathbf{b})$ commute for any $\mathbf{a}$ and $\mathbf{b}$, so that $\Omega(\mathbf{a})\Gamma(\mathbf{b}) = \Gamma(\mathbf{b})\Omega(\mathbf{a})$.

B. Relative Kinematics

In this section a review of the relative quaternion kinematics is shown. The relative attitude, denoted by the quaternion $\mathbf{q}$, which is used to map vectors in the chief frame to vectors in the deputy frame is expressed by

$$\mathbf{q} = \mathbf{q}_d \otimes \mathbf{q}_c^{-1} \tag{22}$$

where $\mathbf{q}_d$ and $\mathbf{q}_c$ are the attitudes with respect to an inertial frame of the chief and deputy spacecraft, respectively. Equation (22) is similar to the error quaternion used in Kalman

filtering. Following Ref. 19, the relative quaternion kinematics can be shown to be given by

$$\dot{\mathbf{q}} = -\begin{bmatrix} [\boldsymbol{\omega}_c\times]\boldsymbol{\varrho} \\ 0 \end{bmatrix} + \frac{1}{2}\begin{bmatrix} (\boldsymbol{\omega}_d - \boldsymbol{\omega}_c) \\ 0 \end{bmatrix} \otimes \mathbf{q} \tag{23}$$

where $\boldsymbol{\omega}_c$ and $\boldsymbol{\omega}_d$ are the angular velocities of the chief and deputy, respectively. Equation (23) is equivalent to the kinematics shown in Ref. 20:

$$\dot{\mathbf{q}} = \frac{1}{2}\Xi(\mathbf{q})\boldsymbol{\omega}_{dc} \tag{24}$$

where $\boldsymbol{\omega}_{dc}$ is the relative angular velocity defined by

$$\boldsymbol{\omega}_{dc} \equiv \boldsymbol{\omega}_d - A(\mathbf{q})\boldsymbol{\omega}_c \tag{25}$$

Equation (24) can be simplified by substituting Eq. (14) into Eq. (25) and using the identities in Eqs. (18), (20b), (20c) and (20f), which yields

$$\dot{\mathbf{q}} = \frac{1}{2}\Theta(\boldsymbol{\omega}_d,\, \boldsymbol{\omega}_c)\mathbf{q} \tag{26}$$

where $\Theta(\boldsymbol{\omega}_d,\, \boldsymbol{\omega}_c) \equiv \Omega(\boldsymbol{\omega}_d) - \Gamma(\boldsymbol{\omega}_c)$.

A closed-form solution for the state transition matrix of $\frac{1}{2}\Theta(\boldsymbol{\omega}_d,\, \boldsymbol{\omega}_c)$ is shown in Ref. 21. As an aside, note that the eigenvalues of this matrix are given by $\pm(||\boldsymbol{\omega}_d|| + ||\boldsymbol{\omega}_c||)j$ and $\pm(||\boldsymbol{\omega}_d|| - ||\boldsymbol{\omega}_c||)j$. Since the matrices $\Omega(\boldsymbol{\omega}_d)$ and $\Gamma(\boldsymbol{\omega}_c)$ commute, we can write

$$\exp\left[\frac{1}{2}\Theta(\boldsymbol{\omega}_d,\, \boldsymbol{\omega}_c)t\right] = \exp\left[\frac{1}{2}\Omega(\boldsymbol{\omega}_d)t\right]\exp\left[-\frac{1}{2}\Gamma(\boldsymbol{\omega}_c)t\right] \tag{27}$$

The closed-form solution for the matrix exponential of $\frac{1}{2}\Omega(\boldsymbol{\omega}_d)t$ is well documented (see

Ref. 22). Applying a similar derivation to the matrix $-\frac{1}{2}\Gamma(\boldsymbol{\omega}_c)t$ gives

$$\exp\left[-\frac{1}{2}\Gamma(\boldsymbol{\omega}_c)t\right] = I_{4\times4}\cos\left(\frac{1}{2}||\boldsymbol{\omega}_c||t\right) - \Gamma(\boldsymbol{\omega}_c)\frac{\sin\left(\frac{1}{2}||\boldsymbol{\omega}_c||t\right)}{||\boldsymbol{\omega}_c||} \tag{28}$$

Hence, the discrete-time propagation of the relative quaternion, assuming that $\boldsymbol{\omega}_c$ and $\boldsymbol{\omega}_d$ are constant over the sampling interval $\Delta t \equiv t_{k+1} - t_k$, is given by

$$\mathbf{q}_{k+1} = \bar{\Omega}(\boldsymbol{\omega}_{d_k})\bar{\Gamma}(\boldsymbol{\omega}_{c_k})\mathbf{q}_k \tag{29}$$

with

$$\bar{\Omega}(\boldsymbol{\omega}_{d_k}) \equiv \begin{bmatrix} \cos\left(\frac{1}{2}||\boldsymbol{\omega}_{d_k}||\,\Delta t\right) I_{3\times3} - [\boldsymbol{\psi}_k\times] & \boldsymbol{\psi}_k \\ -\boldsymbol{\psi}_k^T & \cos\left(\frac{1}{2}||\boldsymbol{\omega}_{d_k}||\,\Delta t\right) \end{bmatrix} \tag{30a}$$

$$\bar{\Gamma}(\boldsymbol{\omega}_{c_k}) \equiv \begin{bmatrix} \cos\left(\frac{1}{2}||\boldsymbol{\omega}_{c_k}||\,\Delta t\right) I_{3\times3} - [\boldsymbol{\zeta}_k\times] & -\boldsymbol{\zeta}_k \\ \boldsymbol{\zeta}_k^T & \cos\left(\frac{1}{2}||\boldsymbol{\omega}_{c_k}||\,\Delta t\right) \end{bmatrix} \tag{30b}$$

where

$$\boldsymbol{\psi}_k \equiv \frac{\sin\left(\frac{1}{2}||\boldsymbol{\omega}_{d_k}||\,\Delta t\right)\boldsymbol{\omega}_{d_k}}{||\boldsymbol{\omega}_{d_k}||} \tag{31a}$$

$$\boldsymbol{\zeta}_k \equiv \frac{\sin\left(\frac{1}{2}||\boldsymbol{\omega}_{c_k}||\,\Delta t\right)\boldsymbol{\omega}_{c_k}}{||\boldsymbol{\omega}_{c_k}||} \tag{31b}$$

Note that the matrices $\bar{\Omega}(\boldsymbol{\omega}_{d_k})$ and $\bar{\Gamma}(\boldsymbol{\omega}_{c_k})$ also commute.

IV. Relative Attitude Estimation

In this section the necessary equations for relative attitude estimation between two spacecraft are derived. The estimator used for this relative estimation is based on the EKF. A review of the EKF equations can be found in Ref. 23. In this section it is assumed that the relative position is known, and only the attitude and gyro biases will be estimated. In the next section, relative position estimation will be implemented as well. Three attitude estimation formulations are presented here. The first estimates the relative attitude and individual gyro biases for the chief and deputy spacecraft. The second estimates the relative attitude, and the relative velocity bias and the deputy gyro bias. The third estimates the relative attitude, and the relative velocity bias and the chief gyro bias.

A. Chief and Deputy Gyro Bias Case

In this section a formulation to estimate the relative attitude, as well as the chief and deputy gyro biases is derived. The truth equations are given by

$$\dot{\mathbf{q}} = \frac{1}{2}\Xi(\mathbf{q})\boldsymbol{\omega}_{dc} \tag{32a}$$

$$\boldsymbol{\omega}_{dc} = \boldsymbol{\omega}_d - A(\mathbf{q})\boldsymbol{\omega}_c \tag{32b}$$

$$\dot{\boldsymbol{\beta}}_c = \boldsymbol{\eta}_{cu} \tag{32c}$$

$$\dot{\boldsymbol{\beta}}_d = \boldsymbol{\eta}_{du} \tag{32d}$$

$$\boldsymbol{\omega}_c = \tilde{\boldsymbol{\omega}}_c - \boldsymbol{\beta}_c - \boldsymbol{\eta}_{cv} \tag{32e}$$

$$\boldsymbol{\omega}_d = \tilde{\boldsymbol{\omega}}_d - \boldsymbol{\beta}_d - \boldsymbol{\eta}_{dv} \tag{32f}$$

The estimates are given by

$$\dot{\hat{\mathbf{q}}} = \frac{1}{2}\Xi(\hat{\mathbf{q}})\hat{\boldsymbol{\omega}}_{dc} \tag{33a}$$

$$\hat{\boldsymbol{\omega}}_{dc} = \hat{\boldsymbol{\omega}}_d - A(\hat{\mathbf{q}})\hat{\boldsymbol{\omega}}_c \tag{33b}$$

$$\dot{\hat{\boldsymbol{\beta}}}_c = \mathbf{0} \tag{33c}$$

$$\dot{\hat{\boldsymbol{\beta}}}_d = \mathbf{0} \tag{33d}$$

$$\hat{\boldsymbol{\omega}}_c = \tilde{\boldsymbol{\omega}}_c - \hat{\boldsymbol{\beta}}_c \tag{33e}$$

$$\hat{\boldsymbol{\omega}}_d = \tilde{\boldsymbol{\omega}}_d - \hat{\boldsymbol{\beta}}_d \tag{33f}$$

The quaternion kinematics involves the attitude matrix. To provide a set of linearized equations used in the covariance propagation in the EKF, we employ the linearization approach shown in Ref. 19. The error quaternion and its derivative are given by

$$\boldsymbol{\delta}\mathbf{q} = \mathbf{q} \otimes \hat{\mathbf{q}}^{-1} \tag{34a}$$

$$\boldsymbol{\delta}\dot{\mathbf{q}} = \dot{\mathbf{q}} \otimes \hat{\mathbf{q}}^{-1} + \mathbf{q} \otimes \dot{\hat{\mathbf{q}}}^{-1} \tag{34b}$$

The derivative of $\hat{\mathbf{q}}^{-1}$ can be derived by taking the derivative of $\hat{\mathbf{q}} \otimes \hat{\mathbf{q}}^{-1} = [0\ 0\ 0\ 1]^T$, which leads to

$$\dot{\hat{\mathbf{q}}}^{-1} = -\frac{1}{2}\hat{\mathbf{q}}^{-1} \otimes \begin{bmatrix} \hat{\boldsymbol{\omega}}_{dc} \\ 0 \end{bmatrix} \tag{35}$$

Substituting Eqs. (32a) and (35) into Eq. (34b) leads to

$$\boldsymbol{\delta}\dot{\mathbf{q}} = \frac{1}{2}\begin{bmatrix} \boldsymbol{\omega}_{dc} \\ 0 \end{bmatrix} \otimes \boldsymbol{\delta}\mathbf{q} - \frac{1}{2}\boldsymbol{\delta}\mathbf{q} \otimes \begin{bmatrix} \hat{\boldsymbol{\omega}}_{dc} \\ 0 \end{bmatrix} \tag{36}$$

Next, we define the following error variables: $\boldsymbol{\delta\omega}_d \equiv \boldsymbol{\omega}_d - \hat{\boldsymbol{\omega}}_d$ and $\boldsymbol{\delta\omega}_c \equiv \boldsymbol{\omega}_c - \hat{\boldsymbol{\omega}}_c$. Using these definitions in $\boldsymbol{\omega}_{dc}$ gives

$$\boldsymbol{\omega}_{dc} = \hat{\boldsymbol{\omega}}_d - A(\mathbf{q})\hat{\boldsymbol{\omega}}_c + \boldsymbol{\delta\omega}_d - A(\mathbf{q})\boldsymbol{\delta\omega}_c \tag{37}$$

The linearization process make the following assumptions, which are valid to within first-order:[19]

$$\boldsymbol{\delta\mathbf{q}} = \begin{bmatrix} \frac{1}{2}\boldsymbol{\delta\alpha} \\ 1 \end{bmatrix} \tag{38a}$$

$$A(\mathbf{q}) = \{I_{3\times 3} - [\boldsymbol{\delta\alpha}\times]\}\, A(\hat{\mathbf{q}}) \tag{38b}$$

where $\boldsymbol{\delta\alpha}$ is a small angle-error correction. Substituting Eq. (38b) into Eq. (37) and neglecting second-order effects leads to

$$\boldsymbol{\omega}_{dc} = \hat{\boldsymbol{\omega}}_{dc} - [A(\hat{\mathbf{q}})\hat{\boldsymbol{\omega}}_c\times]\boldsymbol{\delta\alpha} + \boldsymbol{\delta\omega}_d - A(\hat{\mathbf{q}})\boldsymbol{\delta\omega}_c \tag{39}$$

Substituting Eqs. (38a) and (39) into Eq. (36), and again neglecting second-order effects leads to

$$\boldsymbol{\delta\dot{\alpha}} = -[\hat{\boldsymbol{\omega}}_d\times]\boldsymbol{\delta\alpha} + \boldsymbol{\delta\omega}_d - A(\hat{\mathbf{q}})\boldsymbol{\delta\omega}_c \tag{40}$$

The derivative of the fourth error-quaternion component is zero. Next, using $\boldsymbol{\delta\omega}_d = -(\Delta\boldsymbol{\beta}_d + \boldsymbol{\eta}_{dv})$ and $\boldsymbol{\delta\omega}_c = -(\Delta\boldsymbol{\beta}_c + \boldsymbol{\eta}_{cv})$, where $\Delta\boldsymbol{\beta}_d \equiv \boldsymbol{\beta}_d - \hat{\boldsymbol{\beta}}_d$ and $\Delta\boldsymbol{\beta}_c \equiv \boldsymbol{\beta}_c - \hat{\boldsymbol{\beta}}_c$, in Eq. (40) leads to

$$\boldsymbol{\delta\dot{\alpha}} = -[\hat{\boldsymbol{\omega}}_d\times]\boldsymbol{\delta\alpha} - \Delta\boldsymbol{\beta}_d + A(\hat{\mathbf{q}})\Delta\boldsymbol{\beta}_c + A(\hat{\mathbf{q}})\boldsymbol{\eta}_{cv} - \boldsymbol{\eta}_{dv} \tag{41}$$

The error-state dynamics are now given by

$$\Delta\dot{\mathbf{x}} = F\Delta\mathbf{x} + G\mathbf{w} \tag{42}$$

with

$$\Delta\mathbf{x} \equiv \begin{bmatrix} \boldsymbol{\delta\alpha}^T & \Delta\boldsymbol{\beta}_c^T & \Delta\boldsymbol{\beta}_d^T \end{bmatrix}^T \tag{43a}$$

$$\mathbf{w} \equiv \begin{bmatrix} \boldsymbol{\eta}_{cv}^T & \boldsymbol{\eta}_{dv}^T & \boldsymbol{\eta}_{cu}^T & \boldsymbol{\eta}_{du}^T \end{bmatrix}^T \tag{43b}$$

where

$$F = \begin{bmatrix} -[\hat{\boldsymbol{\omega}}_d\times] & A(\hat{\mathbf{q}}) & -I_{3\times3} \\ 0_{3\times3} & 0_{3\times3} & 0_{3\times3} \\ 0_{3\times3} & 0_{3\times3} & 0_{3\times3} \end{bmatrix} \tag{44a}$$

$$G = \begin{bmatrix} A(\hat{\mathbf{q}}) & -I_{3\times3} & 0_{3\times3} & 0_{3\times3} \\ 0_{3\times3} & 0_{3\times3} & I_{3\times3} & 0_{3\times3} \\ 0_{3\times3} & 0_{3\times3} & 0_{3\times3} & I_{3\times3} \end{bmatrix} \tag{44b}$$

and the spectral density matrix of the process noise $\mathbf{w}$ is given by

$$Q = \begin{bmatrix} \sigma_{cv}^2 I_{3\times3} & 0_{3\times3} & 0_{3\times3} & 0_{3\times3} \\ 0_{3\times3} & \sigma_{dv}^2 I_{3\times3} & 0_{3\times3} & 0_{3\times3} \\ 0_{3\times3} & 0_{3\times3} & \sigma_{cu}^2 I_{3\times3} & 0_{3\times3} \\ 0_{3\times3} & 0_{3\times3} & 0_{3\times3} & \sigma_{du}^2 I_{3\times3} \end{bmatrix} \tag{45}$$

The linearization of the output (measurement) process exactly follows Ref. 19, which is not shown here.

Solutions for the state transition matrix of F and discrete-time process noise covariance are intractable due to the dependence of both on the attitude matrix. A numerical solution is given by van Loan[24] for fixed-parameter systems, which includes a constant sampling interval and time invariant state and covariance matrices. First, the following 18×18 matrix

is formed:

$$\mathcal{A} = \begin{bmatrix} -F & G\,Q\,G^T \\ 0 & F^T \end{bmatrix} \Delta t \tag{46}$$

Then, the matrix exponential of Eq. (46) is computed:

$$\mathcal{B} = e^{\mathcal{A}} \equiv \begin{bmatrix} \mathcal{B}_{11} & \mathcal{B}_{12} \\ 0 & \mathcal{B}_{22} \end{bmatrix} = \begin{bmatrix} \mathcal{B}_{11} & \Phi^{-1}\mathcal{Q} \\ 0 & \Phi^T \end{bmatrix} \tag{47}$$

where Φ is the state transition matrix of F and $\mathcal{Q}$ is the discrete-time covariance matrix. The state transition matrix and discrete-time process noise covariance are then given by

$$\Phi = \mathcal{B}_{22}^T \tag{48a}$$

$$\mathcal{Q} = \Phi\,\mathcal{B}_{12} \tag{48b}$$

If the sampling interval is "small" enough (well within Nyquist's limit), then $\mathcal{Q} = \Delta t\,G\,Q\,G^T$ is a good approximation for the solution given by Eq. (48b).

A summary of the EKF equations for relative attitude estimation is shown in Table 1, where P is the covariance matrix that consists of the covariance of the attitude errors and chief and deputy biases, and the vector $\tilde{\mathbf{y}}$ is given by $\tilde{\mathbf{y}} = [\tilde{\mathbf{b}}_1^T \;\; \tilde{\mathbf{b}}_2^T \;\; \cdots \;\; \tilde{\mathbf{b}}_N^T]^T$. The quaternion is re-normalized after the update stage.[19] A quaternion measurement, denoted by $\tilde{\mathbf{q}}$, which can be computed when at least 4 LOS vectors are available,[25] may be used instead of body vector measurements. Then $\tilde{\mathbf{y}}_k - \mathbf{h}_k(\hat{\mathbf{q}}_k^-)$ is replaced with $2\,\Xi^T(\hat{\mathbf{q}}_k^-)\tilde{\mathbf{q}}_k$. The factor of 2 is required since the angle error is used in the EKF update. Also, $H_k(\hat{\mathbf{q}}_k^-)$ is replaced with $H_k = [I_{3\times3} \;\; 0_{3\times3} \;\; 0_{3\times3}]$ and R_k is replaced with a 3×3 covariance matrix of the attitude errors.

The EKF provides estimates for the individual biases of the chief and deputy, which in turn provide estimates for their respective angular velocities. The relative angular velocity, which is typically used in a controller, such as the one presented in Ref. 20, can be computed using Eq. (33b). The covariance of the relative bias is useful to quantify the expected error

Table 1. Extended Kalman Filter for Relative Attitude Estimation

Initialize	$\hat{\mathbf{q}}(t_0) = \hat{\mathbf{q}}_0, \quad \hat{\boldsymbol{\beta}}_c(t_0) = \hat{\boldsymbol{\beta}}_{c_0} \quad \hat{\boldsymbol{\beta}}_d(t_0) = \hat{\boldsymbol{\beta}}_{d_0}$ $P(t_0) = P_0$
Gain	$K_k = P_k^- H_k^T(\hat{\mathbf{q}}_k^-)[H_k(\hat{\mathbf{q}}_k^-)P_k^- H_k^T(\hat{\mathbf{q}}_k^-) + R_k]^{-1}$ $H_k(\hat{\mathbf{q}}_k^-) = \begin{bmatrix} [A(\hat{\mathbf{q}}^-)\mathbf{r}_1\times] & 0_{3\times3} & 0_{3\times3} \\ \vdots & \vdots & \vdots \\ [A(\hat{\mathbf{q}}^-)\mathbf{r}_N\times] & 0_{3\times3} & 0_{3\times3} \end{bmatrix}\Big\vert_{t_k}$
Update	$P_k^+ = [I - K_k H_k(\hat{\mathbf{q}}_k^-)]P_k^-$ $\Delta\hat{\mathbf{x}}_k^+ = K_k[\tilde{\mathbf{y}}_k - \mathbf{h}_k(\hat{\mathbf{q}}_k^-)]$ $\Delta\hat{\mathbf{x}}_k^+ \equiv \begin{bmatrix} \boldsymbol{\delta\hat{\alpha}}_k^{+T} & \Delta\hat{\boldsymbol{\beta}}_{c_k}^{+T} & \Delta\hat{\boldsymbol{\beta}}_{d_k}^{+T} \end{bmatrix}^T$ $\mathbf{h}_k(\hat{\mathbf{q}}_k^-) = \begin{bmatrix} A(\hat{\mathbf{q}}^-)\mathbf{r}_1 \\ A(\hat{\mathbf{q}}^-)\mathbf{r}_2 \\ \vdots \\ A(\hat{\mathbf{q}}^-)\mathbf{r}_N \end{bmatrix}\Big\vert_{t_k}$ $\hat{\mathbf{q}}_k^+ = \hat{\mathbf{q}}_k^- + \frac{1}{2}\Xi(\hat{\mathbf{q}}_k^-)\boldsymbol{\delta\hat{\alpha}}_k^+$ $\hat{\boldsymbol{\beta}}_{c_k}^+ = \hat{\boldsymbol{\beta}}_{c_k}^- + \Delta\hat{\boldsymbol{\beta}}_{c_k}^+$ $\hat{\boldsymbol{\beta}}_{d_k}^+ = \hat{\boldsymbol{\beta}}_{d_k}^- + \Delta\hat{\boldsymbol{\beta}}_{d_k}^+$
Propagation	$\hat{\boldsymbol{\omega}}_{c_k}^+ = \tilde{\boldsymbol{\omega}}_{c_k} - \hat{\boldsymbol{\beta}}_{c_k}^+$ $\hat{\boldsymbol{\omega}}_{d_k}^+ = \tilde{\boldsymbol{\omega}}_{d_k} - \hat{\boldsymbol{\beta}}_{d_k}^+$ $\hat{\mathbf{q}}_{k+1}^- = \bar{\Omega}(\hat{\boldsymbol{\omega}}_{d_k}^+)\bar{\Gamma}(\hat{\boldsymbol{\omega}}_{c_k}^+)\hat{\mathbf{q}}_k^+$ $P_{k+1}^- = \Phi_k P_k^+ \Phi_k^T + \mathcal{Q}_k$

in the relative velocity estimate. Using the error definitions of the biases and attitude, $\boldsymbol{\beta}_{dc}$ can be expressed by

$$\begin{aligned} \boldsymbol{\beta}_{dc} &= \boldsymbol{\beta}_d - A(\mathbf{q})\,\boldsymbol{\beta}_c \\ &= \left(\hat{\boldsymbol{\beta}}_d + \Delta\boldsymbol{\beta}_d\right) - \{I_{3\times3} - [\boldsymbol{\delta\alpha}\times]\}\,A(\hat{\mathbf{q}})\left(\hat{\boldsymbol{\beta}}_c + \Delta\boldsymbol{\beta}_c\right) \end{aligned} \tag{49}$$

Assuming unbiased estimates gives $E\{\boldsymbol{\beta}_{dc}\} = \hat{\boldsymbol{\beta}}_{dc}$. Next, ignoring second-order effects leads

to

$$\boldsymbol{\beta}_{dc} - \hat{\boldsymbol{\beta}}_{dc} = -[A(\hat{\mathbf{q}})\hat{\boldsymbol{\beta}}_c\times]\boldsymbol{\delta\alpha} - A(\hat{\mathbf{q}})\,\Delta\boldsymbol{\beta}_c + \Delta\boldsymbol{\beta}_d \tag{50}$$

Hence, the covariance of $\boldsymbol{\beta}_{dc}$ is given by

$$\text{cov}\,\{\boldsymbol{\beta}_{dc}\} = \mathcal{H}\,P\,\mathcal{H}^T \tag{51}$$

where

$$\mathcal{H} \equiv \begin{bmatrix} -[A(\hat{\mathbf{q}})\hat{\boldsymbol{\beta}}_c\times] & -A(\hat{\mathbf{q}}) & I_{3\times3} \end{bmatrix} \tag{52}$$

and P is the covariance from the EKF.

B. Relative Velocity and Deputy Gyro Bias Case

In this section a formulation to estimate the relative attitude, as well as the relative velocity and deputy gyro biases is derived. Estimating for the relative bias directly is useful since the EKF gives its covariance directly in this case. Note that Eq. (51) is only valid to within first order and may be inaccurate for large errors. The equations derived in this section and the next are more complicated than the equations used to determine the individual biases of the chief and deputy from the previous section; however, these alternate formulations may be useful in more complex filters designs, such as the Unscented Kalman filter,[26] which retain higher-order terms. The linearized equations must now involve $\hat{\boldsymbol{\beta}}_d$ and $\hat{\boldsymbol{\beta}}_{dc}$. We first derive the attitude-error equation in terms of these variables. Defining $\Delta\boldsymbol{\beta}_{dc} \equiv \boldsymbol{\beta}_{dc} - \hat{\boldsymbol{\beta}}_{dc}$, and using $\hat{\boldsymbol{\beta}}_{dc} = \hat{\boldsymbol{\beta}}_d - A(\hat{\mathbf{q}})\hat{\boldsymbol{\beta}}_c$, $\boldsymbol{\beta}_c = \hat{\boldsymbol{\beta}}_c + \Delta\boldsymbol{\beta}_c$ and Eq. (38b) leads to

$$\Delta\boldsymbol{\beta}_{dc} = [(\hat{\boldsymbol{\beta}}_{dc} - \hat{\boldsymbol{\beta}}_d)\times]\boldsymbol{\delta\alpha} + \Delta\boldsymbol{\beta}_d - A(\hat{\mathbf{q}})\Delta\boldsymbol{\beta}_c \tag{53}$$

where second-order effects are ignored. Solving Eq. (53) for $A(\hat{\mathbf{q}})\Delta\boldsymbol{\beta}_c - \Delta\boldsymbol{\beta}_d$ and substituting the resultant into Eq. (41) leads to

$$\boldsymbol{\delta\dot{\alpha}} = -[(\tilde{\boldsymbol{\omega}}_d - \hat{\boldsymbol{\beta}}_{dc})\times]\boldsymbol{\delta\alpha} - \Delta\boldsymbol{\beta}_{dc} + A(\hat{\mathbf{q}})\boldsymbol{\eta}_{cv} - \boldsymbol{\eta}_{dv} \tag{54}$$

Next, we need to determine a dynamics model for $\boldsymbol{\beta}_{dc} = \boldsymbol{\beta}_d - A(\mathbf{q})\boldsymbol{\beta}_c$. Taking the time derivative of this equation and using Eqs. (32b)-(32f) in the resulting expression yields

$$\begin{aligned}\dot{\boldsymbol{\beta}}_{dc} = &-[(\tilde{\boldsymbol{\omega}}_d - A(\mathbf{q})\tilde{\boldsymbol{\omega}}_c - \boldsymbol{\beta}_d - \boldsymbol{\eta}_{dv} + A(\mathbf{q})\boldsymbol{\eta}_{cv})\times]\boldsymbol{\beta}_{dc} \\ &+ [(\tilde{\boldsymbol{\omega}}_d - A(\mathbf{q})\tilde{\boldsymbol{\omega}}_c - \boldsymbol{\eta}_{dv} + A(\mathbf{q})\boldsymbol{\eta}_{cv})\times]\boldsymbol{\beta}_d + \boldsymbol{\eta}_{du} - A(\mathbf{q})\boldsymbol{\eta}_{cu}\end{aligned} \tag{55}$$

The estimate equation is given by

$$\dot{\hat{\boldsymbol{\beta}}}_{dc} = -[(\tilde{\boldsymbol{\omega}}_d - A(\hat{\mathbf{q}})\tilde{\boldsymbol{\omega}}_c - \hat{\boldsymbol{\beta}}_d)\times]\hat{\boldsymbol{\beta}}_{dc} + [(\tilde{\boldsymbol{\omega}}_d - A(\hat{\mathbf{q}})\tilde{\boldsymbol{\omega}}_c)\times]\hat{\boldsymbol{\beta}}_d \tag{56}$$

The linear dynamics of $\Delta\dot{\boldsymbol{\beta}}_{dc}$ can be derived in a similar fashion as the other linearized equations shown to this point. For brevity this derivation is omitted here. The error-state dynamics are given by

$$\Delta\dot{\mathbf{x}} = F\Delta\mathbf{x} + G\mathbf{w} \tag{57}$$

with

$$\Delta\mathbf{x} \equiv \begin{bmatrix}\boldsymbol{\delta\alpha}^T & \Delta\boldsymbol{\beta}_{dc}^T & \Delta\boldsymbol{\beta}_d^T\end{bmatrix}^T \tag{58a}$$

$$\mathbf{w} \equiv \begin{bmatrix}\boldsymbol{\eta}_{cv}^T & \boldsymbol{\eta}_{dv}^T & \boldsymbol{\eta}_{cu}^T & \boldsymbol{\eta}_{du}^T\end{bmatrix}^T \tag{58b}$$

where

$$F = \begin{bmatrix} -[(\tilde{\boldsymbol{\omega}}_d - \hat{\boldsymbol{\beta}}_{dc})\times] & -I_{3\times3} & 0_{3\times3} \\ F_{21} & F_{22} & F_{23} \\ 0_{3\times3} & 0_{3\times3} & 0_{3\times3} \end{bmatrix} \tag{59a}$$

$$F_{21} = [(\hat{\boldsymbol{\beta}}_d - \hat{\boldsymbol{\beta}}_{dc})\times][A(\hat{\mathbf{q}})\tilde{\boldsymbol{\omega}}_c\times] \tag{59b}$$

$$F_{22} = -[(\tilde{\boldsymbol{\omega}}_d - A(\hat{\mathbf{q}})\tilde{\boldsymbol{\omega}}_c - \hat{\boldsymbol{\beta}}_d)\times] \tag{59c}$$

$$F_{23} = [(\tilde{\boldsymbol{\omega}}_d - A(\hat{\mathbf{q}})\tilde{\boldsymbol{\omega}}_c - \hat{\boldsymbol{\beta}}_{dc})\times] \tag{59d}$$

$$G = \begin{bmatrix} A(\hat{\mathbf{q}}) & -I_{3\times3} & 0_{3\times3} & 0_{3\times3} \\ -[(\hat{\boldsymbol{\beta}}_d - \hat{\boldsymbol{\beta}}_{dc})\times]A(\hat{\mathbf{q}}) & [(\hat{\boldsymbol{\beta}}_d - \hat{\boldsymbol{\beta}}_{dc})\times] & -A(\hat{\mathbf{q}}) & I_{3\times3} \\ 0_{3\times3} & 0_{3\times3} & 0_{3\times3} & I_{3\times3} \end{bmatrix} \tag{59e}$$

and the spectral density matrix of the process noise $\mathbf{w}$ is given by Eq. (45). The EKF filter equations can now be employed using the state matrices in Eq. (57) in the covariance propagation as well as Eqs. (33a), (33d) and (56) for the state propagation.

C. Relative Velocity and Chief Gyro Bias Case

In this section the necessary equations to estimate the relative attitude, as well as the relative velocity and chief gyro biases are shown. For brevity these equations are shown without derivation. The dynamic equation for the relative bias estimate is given by

$$\dot{\hat{\boldsymbol{\beta}}}_{dc} = [A(\hat{\mathbf{q}})\hat{\boldsymbol{\beta}}_c\times]\hat{\boldsymbol{\beta}}_{dc} - [A(\hat{\mathbf{q}})\hat{\boldsymbol{\beta}}_c\times](\tilde{\boldsymbol{\omega}}_d - A(\hat{\mathbf{q}})\tilde{\boldsymbol{\omega}}_c) \tag{60}$$

The error-state dynamics are given by

$$\Delta\dot{\mathbf{x}} = F\Delta\mathbf{x} + G\mathbf{w} \tag{61}$$

with

$$\Delta\mathbf{x} \equiv \begin{bmatrix} \boldsymbol{\delta\alpha}^T & \Delta\boldsymbol{\beta}_{dc}^T & \Delta\boldsymbol{\beta}_{c}^T \end{bmatrix}^T \tag{62a}$$

$$\mathbf{w} \equiv \begin{bmatrix} \boldsymbol{\eta}_{cv}^T & \boldsymbol{\eta}_{dv}^T & \boldsymbol{\eta}_{cu}^T & \boldsymbol{\eta}_{du}^T \end{bmatrix}^T \tag{62b}$$

where

$$F = \begin{bmatrix} -[(\tilde{\boldsymbol{\omega}}_d - \hat{\boldsymbol{\beta}}_{dc})\times] & -I_{3\times3} & 0_{3\times3} \\ F_{21} & F_{22} & F_{23} \\ 0_{3\times3} & 0_{3\times3} & 0_{3\times3} \end{bmatrix} \tag{63a}$$

$$F_{21} = [A(\hat{\mathbf{q}})\hat{\boldsymbol{\beta}}_c\times][A(\hat{\mathbf{q}})\tilde{\boldsymbol{\omega}}_c\times] + [(\tilde{\boldsymbol{\omega}}_d - A(\hat{\mathbf{q}})\tilde{\boldsymbol{\omega}}_c - \hat{\boldsymbol{\beta}}_{dc})\times][A(\hat{\mathbf{q}})\hat{\boldsymbol{\beta}}_c\times] \tag{63b}$$

$$F_{22} = [A(\hat{\mathbf{q}})\hat{\boldsymbol{\beta}}_c\times] \tag{63c}$$

$$F_{23} = [(\tilde{\boldsymbol{\omega}}_d - A(\hat{\mathbf{q}})\tilde{\boldsymbol{\omega}}_c - \hat{\boldsymbol{\beta}}_{dc})\times]A(\hat{\mathbf{q}}) \tag{63d}$$

$$G = \begin{bmatrix} A(\hat{\mathbf{q}}) & -I_{3\times3} & 0_{3\times3} & 0_{3\times3} \\ -[A(\hat{\mathbf{q}})\hat{\boldsymbol{\beta}}_c\times]A(\hat{\mathbf{q}}) & [A(\hat{\mathbf{q}})\hat{\boldsymbol{\beta}}_c\times] & -A(\hat{\mathbf{q}}) & I_{3\times3} \\ 0_{3\times3} & 0_{3\times3} & I_{3\times3} & 0_{3\times3} \end{bmatrix} \tag{63e}$$

and the spectral density matrix of the process noise $\mathbf{w}$ is again given by Eq. (45). The EKF filter equations can now be employed using the state matrices in Eq. (61) in the covariance propagation as well as Eqs. (33a), (33c) and (60) for the state propagation.

V. Relative Attitude and Position Estimation

In this section the necessary equations for both relative attitude and position estimation between two spacecraft are derived. The state vector in the attitude-only estimation formulations shown in the previous section is now appended to include relative position and velocity of the deputy, radius and radial rate of the chief, and the true anomaly and its rate.

This appended vector is given by

$$\begin{aligned}\mathbf{X} &= \begin{bmatrix} x & y & z & \dot{x} & \dot{y} & \dot{z} & r_c & \dot{r}_c & \theta & \dot{\theta} \end{bmatrix}^T \\ &\equiv \begin{bmatrix} x_1 & x_2 & x_3 & x_4 & x_5 & x_6 & x_7 & x_8 & x_9 & x_{10} \end{bmatrix}^T \end{aligned} \tag{64}$$

The nonlinear state-space model follows from Eqs. (1) and (2) as

$$\dot{\mathbf{X}} = \mathbf{f}(\mathbf{X}) \equiv \begin{bmatrix} x_4 \\ x_5 \\ x_6 \\ x_1 x_{10}^2 \left(1 + 2x_7/p\right) + 2x_{10}\left(x_5 - x_2 x_8/x_7\right) \\ -2x_{10}\left(x_4 - x_1 x_8/x_7\right) + x_2 x_{10}^2 \left(1 - x_7/p\right) \\ -x_7 x_{10}^2 x_3/p \\ x_8 \\ x_7 x_{10}^2 \left(1 - x_7/p\right) \\ x_{10} \\ -2x_8 x_{10}/x_7 \end{bmatrix} \tag{65}$$

Here it is assumed that p is known perfectly. Any error in p can be incorporated into the process noise vector if needed. The full state vector is now given by

$$\mathbf{x} \equiv \begin{bmatrix} \mathbf{q}^T & \boldsymbol{\beta}_c^T & \boldsymbol{\beta}_d^T & \mathbf{X}^T \end{bmatrix}^T \tag{66}$$

The error-state vector for the chief and deputy gyro bias case is now given by

$$\Delta\mathbf{x} \equiv \begin{bmatrix} \boldsymbol{\delta\alpha}^T & \Delta\boldsymbol{\beta}_c^T & \Delta\boldsymbol{\beta}_d^T & \Delta\boldsymbol{\rho}^T & \Delta\dot{\boldsymbol{\rho}}^T & \Delta r_c & \Delta\dot{r}_c & \Delta\theta & \Delta\dot{\theta} \end{bmatrix}^T \tag{67}$$

with obvious definitions of $\Delta\boldsymbol{\rho}$, $\dot{\boldsymbol{\rho}}$, Δr_c, $\Delta\dot{r}_c$, $\Delta\theta$ and $\Delta\dot{\theta}$. The matrices F and G that are used in the EKF covariance propagation are given by

$$F = \begin{bmatrix} -[\hat{\boldsymbol{\omega}}_d\times] & A(\hat{\mathbf{q}}) & -I_{3\times3} & 0_{3\times10} \\ 0_{3\times3} & 0_{3\times3} & 0_{3\times3} & 0_{3\times10} \\ 0_{3\times3} & 0_{3\times3} & 0_{3\times3} & 0_{3\times10} \\ 0_{10\times3} & 0_{10\times3} & 0_{10\times3} & \frac{\partial\mathbf{f}(\mathbf{X})}{\partial\mathbf{X}}\Big|_{\hat{\mathbf{X}}} \end{bmatrix} \tag{68a}$$

$$G = \begin{bmatrix} A(\hat{\mathbf{q}}) & -I_{3\times3} & 0_{3\times3} & 0_{3\times3} & 0_{3\times3} \\ 0_{3\times3} & 0_{3\times3} & I_{3\times3} & 0_{3\times3} & 0_{3\times3} \\ 0_{3\times3} & 0_{3\times3} & 0_{3\times3} & I_{3\times3} & 0_{3\times3} \\ 0_{3\times3} & 0_{3\times3} & 0_{3\times3} & 0_{3\times3} & 0_{3\times3} \\ 0_{3\times3} & 0_{3\times3} & 0_{3\times3} & 0_{3\times3} & I_{3\times3} \\ 0_{2\times3} & 0_{2\times3} & 0_{2\times3} & 0_{2\times3} & 0_{2\times3} \\ 0_{2\times3} & 0_{2\times3} & 0_{2\times3} & 0_{2\times3} & 0_{2\times3} \end{bmatrix} \tag{68b}$$

where $\hat{\mathbf{X}}$ denotes the estimate of $\mathbf{X}$. The partial matrix $\partial\mathbf{f}(\mathbf{X})/\partial\mathbf{X}$ is straightforward to derive and is not shown here for brevity. Defining the new process noise vector as $\mathbf{w} \equiv \begin{bmatrix}\boldsymbol{\eta}_{cv}^T & \boldsymbol{\eta}_{dv}^T & \boldsymbol{\eta}_{cu}^T & \boldsymbol{\eta}_{du}^T & w_x & w_y & w_z\end{bmatrix}^T$, then the new matrix Q is given by

$$Q = \begin{bmatrix} \sigma_{cv}^2 I_{3\times3} & 0_{3\times3} & 0_{3\times3} & 0_{3\times3} & 0_{3\times1} & 0_{3\times1} & 0_{3\times1} \\ 0_{3\times3} & \sigma_{dv}^2 I_{3\times3} & 0_{3\times3} & 0_{3\times3} & 0_{3\times1} & 0_{3\times1} & 0_{3\times1} \\ 0_{3\times3} & 0_{3\times3} & \sigma_{cu}^2 I_{3\times3} & 0_{3\times3} & 0_{3\times1} & 0_{3\times1} & 0_{3\times1} \\ 0_{3\times3} & 0_{3\times3} & 0_{3\times3} & \sigma_{du}^2 I_{3\times3} & 0_{3\times1} & 0_{3\times1} & 0_{3\times1} \\ 0_{1\times3} & 0_{1\times3} & 0_{1\times3} & 0_{1\times3} & \sigma_x^2 & 0 & 0 \\ 0_{1\times3} & 0_{1\times3} & 0_{1\times3} & 0_{1\times3} & 0 & \sigma_y^2 & 0 \\ 0_{1\times3} & 0_{1\times3} & 0_{1\times3} & 0_{1\times3} & 0 & 0 & \sigma_z^2 \end{bmatrix} \tag{69}$$

The sensitivity matrix is modified to be

$$H_k(\hat{\mathbf{q}}_k^-,\, \hat{\boldsymbol{\rho}}_k^-) = \left[\begin{array}{ccccc} [A(\hat{\mathbf{q}}^-)\hat{\mathbf{r}}_1^-\times] & 0_{3\times3} & 0_{3\times3} & \dfrac{\partial\hat{\mathbf{b}}_1^-}{\partial\hat{\boldsymbol{\rho}}^-} & 0_{3\times7} \\ \vdots & \vdots & \vdots & \vdots & \vdots \\ [A(\hat{\mathbf{q}}^-)\hat{\mathbf{r}}_N^-\times] & 0_{3\times3} & 0_{3\times3} & \dfrac{\partial\hat{\mathbf{b}}_N^-}{\partial\hat{\boldsymbol{\rho}}^-} & 0_{3\times7} \end{array}\right]\Bigg|_{t_k} \tag{70}$$

where $\hat{\mathbf{r}}_i^-$ is given by Eq. (6b) evaluated at $\hat{\boldsymbol{\rho}}^- \equiv [\hat{x}^- \;\; \hat{y}^- \;\; \hat{z}^-]^T$ and the partial matrix $\partial\hat{\mathbf{b}}_i^-/\partial\hat{\boldsymbol{\rho}}^-$ is given by

$$\frac{\partial\hat{\mathbf{b}}_i^-}{\partial\hat{\boldsymbol{\rho}}^-} = A(\hat{\mathbf{q}}^-)\frac{\partial\hat{\mathbf{r}}_i^-}{\partial\hat{\boldsymbol{\rho}}^-} \tag{71}$$

where

$$\frac{\partial\hat{\mathbf{r}}_i^-}{\partial\hat{\boldsymbol{\rho}}^-} = \frac{1}{\hat{s}_i^-}\left[\begin{array}{ccc} -[(Y_i-\hat{y}^-)^2+(Z_i-\hat{z}^-)^2] & (X_i-\hat{x}^-)(Y_i-\hat{y}^-) & (X_i-\hat{x}^-)(Z_i-\hat{z}^-) \\ (X_i-\hat{x}^-)(Y_i-\hat{y}^-) & -[(X_i-\hat{x}^-)^2+(Z_i-\hat{z}^-)^2] & (Y_i-\hat{y}^-)(Z_i-\hat{z}^-) \\ (X_i-\hat{x}^-)(Z_i-\hat{z}^-) & (Y_i-\hat{y}^-)(Z_i-\hat{z}^-) & -[(X_i-\hat{x}^-)^2+(Y_i-\hat{y}^-)^2] \end{array}\right] \tag{72}$$

with $\hat{s}_i^- \equiv [(X_i-\hat{x}^-)^2+(Y_i-\hat{y}^-)^2+(Z_i-\hat{z}^-)^2]^{3/2}$. The EKF can now be executed with these new quantities to estimate both relative attitude and position. In the formulation of this section the chief radius and true anomaly, as well as their respective derivatives, are estimated. The observability of these quantities from relative position measurements is discussed in Refs. 27 and 28. If this information is assumed known *a priori*, then these states can removed and their respective measured values can be added as process noise in the state model.

VI. Simulation Results

In this section simulation results are presented that show the performance of the EKF to estimate both relative attitude and position between spacecraft. For the chief spacecraft, parameters from the Hubble Space Telescope are selected. The semimajor axis is given by

6,998,455 meters and the eccentricity is $e = 0.00172$. A bounded relative orbit is used. The constraint required on the Cartesian initial conditions must then satisfy[11]

$$\frac{\dot{y}(t_0)}{x(t_0)} = \frac{-n(2+e)}{\sqrt{(1+e)(1-e)^3}} \tag{73}$$

This bounded relative orbit constraint is valid for both eccentric and circular chief orbits. Note that its form requires that t_0 be defined to be at the orbit perigee point. This is only used for simulation purposes though. The EKF can be initiated at any part of the orbit. The initial chief orbit radius and true anomaly rate are given by $r_c(t_0) = a(1-e)$ and $\dot{\theta}(t_0) = \sqrt{\mu/p}\,(1+e)/r_c$, where $\mu = 3.986008 \times 10^{14}$ m^3/s^2. At perigee we have $\dot{r}_c(t_0) = 0$ and $\theta(t_0) = 0$. The initial condition for the vector $\mathbf{X}$ in appropriate units of meters and meters per second is given by

$$\mathbf{X}(t_0) = \begin{bmatrix} 200 & 200 & 100 & 0.01 & -0.4325 & 0.01 & r_c(t_0) & 0 & 0 & \dot{\theta}(t_0) \end{bmatrix}^T \tag{74}$$

The simulation time for relative motion between the two spacecraft is 600 minutes and the update rate for all of the sensors is 10 seconds. The spectral densities of the process noise components w_x, w_y and w_z in Eq. (1) are each given by $\sqrt{10} \times 10^{-11}$ m/(s$\sqrt{\text{s}}$). The relative orbit period of the deputy is calculated to be 5,820 seconds. This period makes the deputy move about 6 times around the chief during the simulation run.

The true relative attitude motion is given by propagating Eq. (29) using an initial quaternion given by $\mathbf{q}(t_0) = [\sqrt{2}/2 \;\; 0 \;\; 0 \;\; \sqrt{2}/2]^T$ and angular velocities given by $\boldsymbol{\omega}_c = [0 \;\; 0.0011 \;\; -0.0011]^T$ rad/sec and $\boldsymbol{\omega}_d = [-0.002 \;\; 0 \;\; 0.0011]^T$ rad/sec for the entire simulation run. The gyro noise parameters are given by $\sigma_{cu} = \sigma_{du} = \sqrt{10} \times 10^{-10}$ rad/sec$^{3/2}$ and $\sigma_{cv} = \sigma_{dv} = \sqrt{10} \times 10^{-5}$ rad/sec$^{1/2}$. The initial biases for each axis of both the chief and

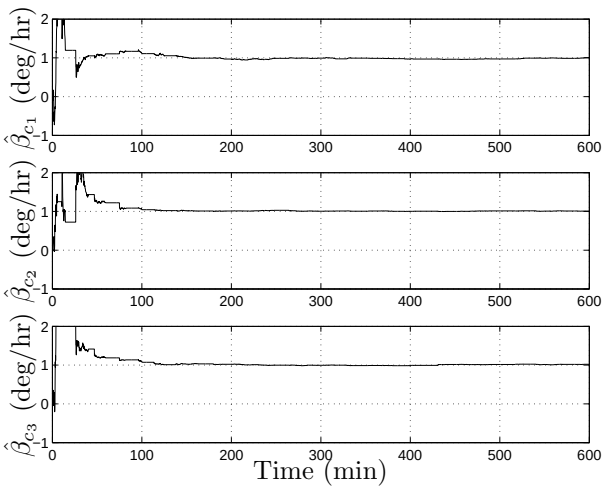

(a) Chief Bias Estimates

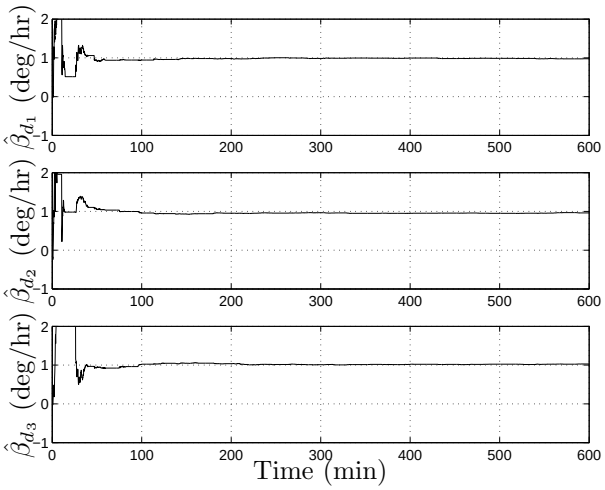

(b) Deputy Bias Estimates

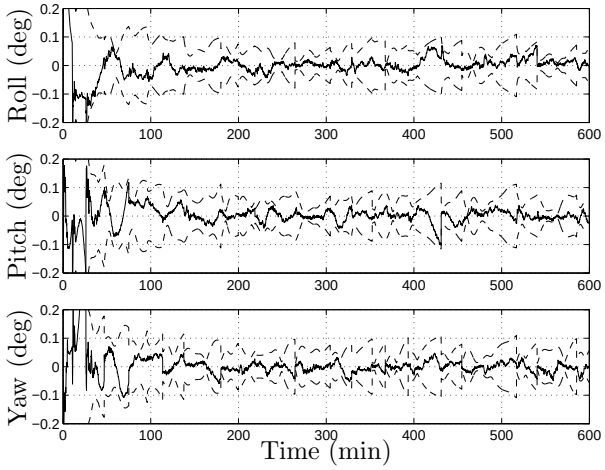

(c) Attitude Errors and 3σ Bounds

Figure 3. Gyro Bias Estimates and Attitude Errors

deputy gyros are given by 1 deg/hr. Six beacons are assumed to exist on the chief:

$$X_1 = 0.5\text{m}, \quad Y_1 = 0.5\text{m}, \quad Z_1 = 0.0\text{m} \tag{75a}$$

$$X_2 = -0.5\text{m}, \quad Y_2 = -0.5\text{m}, \quad Z_2 = 0.0\text{m} \tag{75b}$$

$$X_3 = -0.5\text{m}, \quad Y_3 = 0.5, \quad Z_3 = 0.0\text{m} \tag{75c}$$

$$X_4 = 0.5\text{m}, \quad Y_4 = -0.5\text{m}, \quad Z_4 = 0.0\text{m} \tag{75d}$$

$$X_5 = 0.2\text{m}, \quad Y_5 = 0.5\text{m}, \quad Z_5 = 0.1\text{m} \tag{75e}$$

$$X_6 = 0.0\text{m}, \quad Y_6 = 0.2\text{m}, \quad Z_6 = -0.1\text{m} \tag{75f}$$

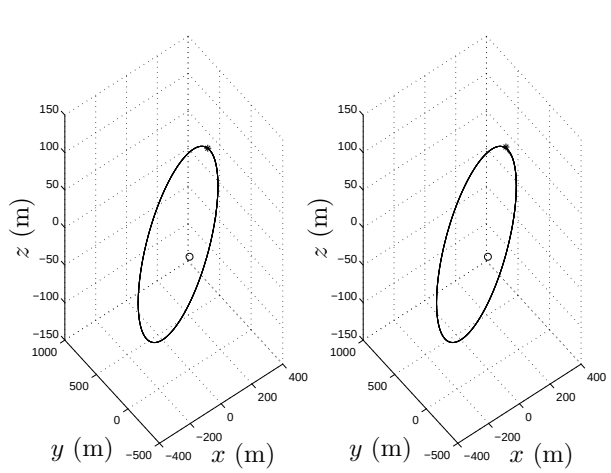

(a) True and Estimated Position Comparison

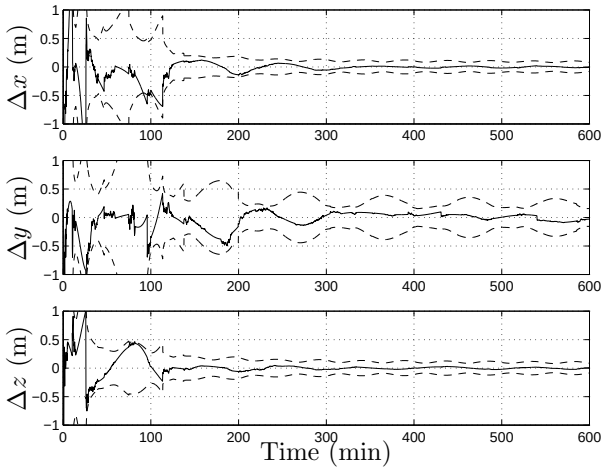

(b) Position Errors and 3σ Bounds

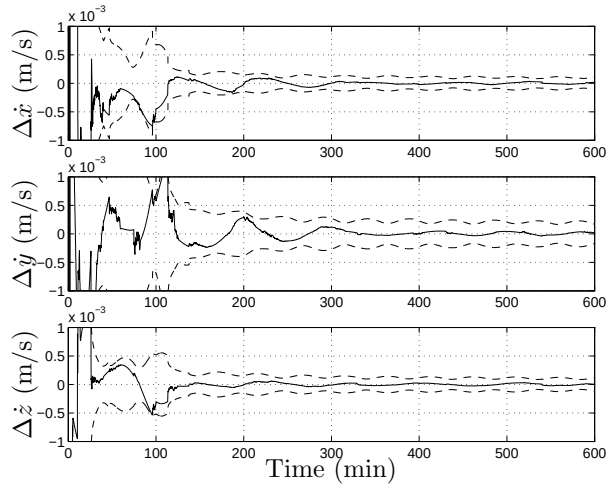

(c) Velocity Errors and 3σ Bounds

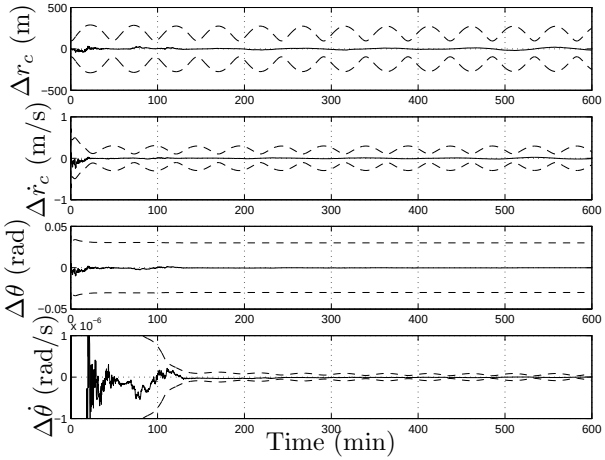

(d) Chief Orbit Element Errors and 3σ Bounds

Figure 4. Orbit Element Estimates

In order to provide a realistic simulation, measurement updates in the filter are only used when the beacons are within the FOV of the sensor. Simulated VISNAV measurements are generated using Eq. (7) with a measurement standard deviation given by $\sigma_i = 0.0005$ degrees.

In order to initialize the EKF a nonlinear least squares routine from the synthetic measurements is used to determine the initial relative attitude and position. This corresponds to an initial attitude error of about 3 degrees (3σ) and an initial position error of about 6

meters (3σ) for each axis. The initial velocity and gyro biases are all set to zero for the filter, and the initial chief orbit elements are given by their respected true values. Each individual covariance sub-matrix for the attitude, gyro biases, position and velocity is assumed to be initially isotropic, i.e. a diagonal matrix with equal elements. The initial attitude covariance is given by $I_{3\times3}$ deg^2. The initial chief and deputy gyro bias covariances are each set to $4I_{3\times3}$ (deg/hr)^2. The initial position covariance is set to $5I_{3\times3}$ m^2 and the initial velocity covariance is set to $0.02I_{3\times3}$ (m/s)^2. The initial variance for the chief position is set to 1,000 m^2 and the velocity variance is set to 0.01 (m/s)^2. The initial variance for the true anomaly is set to 1×10^{-4} rad^2 and the rate variance is set to 1×10^{-4} (rad/sec)^2.

Figures 3(a) and 3(b) show the chief and deputy bias estimates, which are all well estimated by the EKF. Figure 3(c) shows the attitude errors and respective 3σ bounds derived from the EKF covariance matrix. All errors remain within their respective bounds, which indicates that the EKF is working properly. The attitude errors are within 0.1 degrees. Figure 4(a) shows a comparison between the true and estimated position, with the errors shown in Figure 4(b). Relative position knowledge is within 0.4 meters for each axis. Figure 4(c) shows the relative velocity errors, which shows that velocity knowledge is within 3×10^{-4} meters per second. The chief orbital element errors are shown in Figure 4(d). The chief radius has a maximum 3σ bound of about 300 meters, although the actual errors are much smaller. The velocity errors are well below 1 meter per second. The true anomaly 3σ bound shows that its estimate error may be fairly large, up to about 2 degrees, although the actual errors are much smaller. The true anomaly rate is known to within 1×10^{-7} rad/sec.

The accuracy of these estimates not only depends on the accuracy of the PSD sensor and the number of beacons, but also on the "spread" of the beacons as well as the distance from the beacons and PSD. From Figures 3(c) and 4(b) the attitude and position covariance increases just past 60 minutes, which intuitively makes sense since this coincides with the maximum relative distance between the spacecraft. It is again important to note that the filter developed in this paper estimates not only the deputy states, but also the chief states including the chief radius, true anomaly and gyro biases. In actual practice, the chief

parameters will be known through external sensors onboard the chief spacecraft. For this more practical case, the states in the filter design presented here can be reduced to only deputy-associated parameters.

VII. Conclusions

An extended Kalman filter has been designed for relative attitude and position estimation for spacecraft formation flying applications. The measurements were assumed to be given by line-of-sight observations and gyro measurements from the chief and deputy spacecraft. For attitude estimation three different filter formulations were presented. The first directly estimated the chief and deputy gyro biases. The second estimated the relative velocity and deputy gyro biases, and the third estimated the relative velocity and chief gyro biases. For position estimation a nonlinear orbital model was used, where errors and disturbances were modeled by process noise. Simulation results have shown that the combined relative attitude/position Kalman filter is able to achieve accurate results using a close configuration of beacons with a modest relative distance between spacecraft.

References

[1]Robertson, A., Corazzini, T., LeMaster, F., and How, J. P., "Formation Sensing and Control Technologies for a Separated Spacecraft Interferometer," *Proceedings of the 1998 American Control Conference*, Philadelphia, PA, June 1998, pp. 1574–1580.

[2]Carpenter, J., Leitner, J., Folta, D., and Burns, R., "Benchmark Problems for Spacecraft Formation Flying Missions," *AIAA Guidance, Navigation, and Control Conference*, Austin, TX, Aug. 2003, AIAA-2003-5364.

[3]Corazzini, T., Robertson, A., Adams, J. C., Hassibi, A., and How, J. P., "GPS Sensing for Spacecraft Formation Flying," *ION-GPS-97 Conference*, Kansas, MO, Sept. 1997, pp. 735–744.

[4]Purcell, G., Kuang, D., Lichten, S., Wu, S. C., and Young, L., "Autonomous Formation Flyer (AFF) Sensor Technology Development," *AAS Guidance and Control Conference*, Breckenridge, CO, Feb. 1998, AAS-98-062.

[5]Gunnam, K. K., Hughes, D. C., Junkins, J. L., and Kehtarnavaz, N., "A Vision-Based DSP Embedded

Navigation Sensor," *IEEE Sensors Journal*, Vol. 2, No. 5, Oct. 2002, pp. 428–442.

[6]Hill, G., "Researches in the Lunar Theory," *American Journal of Mathematics*, Vol. 1, 1878, pp. 5–26.

[7]Clohessy, W. and Wiltshire, R., "Terminal Guidance System for Satellite Rendezvous," *Journal of the Aerospace Sciences*, Vol. 27, No. 9, Sept. 1960, pp. 653–658.

[8]Inalhan, G., Tillerson, M., and How, J. P., "Relative Dynamics and Control of Spacecraft Formations in Eccentric Orbits," *Journal of Guidance, Control, and Dynamics*, Vol. 25, No. 1, Jan.-Feb. 2002, pp. 48–59.

[9]Alfriend, K. T., Yan, H., and Vadali, S. R., "Nonlinear Considerations in Satellite Formation Flying," *AIAA/AAS Astrodynamics Specialist Conference*, Monterey, CA, Aug. 2002, AIAA-2002-4741.

[10]Karlgaard, C. D. and Lutze, F. H., "Second-Order Relative Motion Equations," *AAS/AIAA Astrodynamics Specialist Conference*, Quebec City, Canada, July 2001, AAS-01-464.

[11]Schaub, H. and Junkins, J. L., *Analytical Mechanics of Aerospace Systems*, chap. 14, American Institute of Aeronautics and Astronautics, Inc., New York, NY, 2003.

[12]Ju, G., Pollack, T., and Junkins, J. L., "DIGISTAR II Micro-Star Tracker: Autonomous On-Orbit Calibration and Attitude Estimation," *AAS/AIAA Astrodynamics Specialist Conference*, Girdwood, AK, Aug. 1999, AAS-99-431.

[13]Light, D. L., "Satellite Photogrammetry," *Manual of Photogrammetry*, edited by C. C. Slama, chap. 17, American Society of Photogrammetry, Falls Church, VA, 4th ed., 1980.

[14]Cheng, Y., Crassidis, J. L., and Markley, F. L., "Attitude Estimation for Large Field-of-View Sensors," *AAS Malcolm D. Shuster Astronautics Symposium*, Grand Island, NY, June 2005, AAS-05-462.

[15]Shuster, M. D., "Kalman Filtering of Spacecraft Attitude and the QUEST Model," *The Journal of the Astronautical Sciences*, Vol. 38, No. 3, July-Sept. 1990, pp. 377–393.

[16]Shuster, M. D. and Oh, S. D., "Three-Axis Attitude Determination from Vector Observations," *Journal of Guidance and Control*, Vol. 4, No. 1, Jan.-Feb. 1981, pp. 70–77.

[17]Farrenkopf, R. L., "Analytic Steady-State Accuracy Solutions for Two Common Spacecraft Attitude Estimators," *Journal of Guidance and Control*, Vol. 1, No. 4, July-Aug. 1978, pp. 282–284.

[18]Shuster, M. D., "A Survey of Attitude Representations," *Journal of the Astronautical Sciences*, Vol. 41, No. 4, Oct.-Dec. 1993, pp. 439–517.

[19]Lefferts, E. J., Markley, F. L., and Shuster, M. D., "Kalman Filtering for Spacecraft Attitude Estimation," *Journal of Guidance, Control, and Dynamics*, Vol. 5, No. 5, Sept.-Oct. 1982, pp. 417–429.

[20]Xing, G. Q. and Parvez, S. A., "Nonlinear Attitude State Tracking Control for Spacecraft," *Journal of Guidance, Control, and Dynamics*, Vol. 24, No. 3, May-June 2001, pp. 624–626.

[21]Mayo, R. A., "Relative Quaternion State Transition Relation," *Journal of Guidance and Control*, Vol. 2, No. 1, Jan.-Feb. 1979, pp. 44–48.

[22]Markley, F. L., "Matrix and Vector Algebra," *Spacecraft Attitude Determination and Control*, edited by J. R. Wertz, appendix C, Kluwer Academic Publishers, The Netherlands, 1978, p. 755.

[23]Crassidis, J. L. and Junkins, J. L., *Optimal Estimation of Dynamic Systems*, chap. 7, Chapman & Hall/CRC, Boca Raton, FL, 2004.

[24]van Loan, C. F., "Computing Integrals Involving the Matrix Exponential," *IEEE Transactions on Automatic Control*, Vol. AC-23, No. 3, June 1978, pp. 396–404.

[25]Sun, D. and Crassidis, J. L., "Observability Analysis of Six-Degree-of-Freedom Configuration Determination Using Vector Observations," *Journal of Guidance, Control, and Dynamics*, Vol. 25, No. 6, Nov.-Dec. 2002, pp. 1149–1157.

[26]Crassidis, J. L. and Markley, F. L., "Unscented Filtering for Spacecraft Attitude Estimation," *Journal of Guidance, Control, and Dynamics*, Vol. 26, No. 4, 2003, pp. 536–542.

[27]Markley, F. L., "Autonomous Navigation Using Landmark and Intersatellite Data," *AIAA/AAS Astrodynamics Conference*, Seattle, WA, Aug. 1984, AIAA-1984-1987.

[28]Psiaki, M. L., "Autonomous Orbit Determination for Two Spacecraft from Relative Position Measurements," *Journal of Guidance, Control, and Dynamics*, Vol. 22, No. 2, March-April 1999, pp. 305–312.